The Indian Ocean Forecast System

P. A. Francis[1], P. N. Vinayachandran[2] and S. S. C. Shenoi[1,*]

[1]Indian National Centre for Ocean Information Services, Hyderabad 500 090, India
[2]Centre for Atmospheric and Oceanic Sciences, Indian Institute of Science, Bangalore 560 012, India

In order to meet the ever growing demand for the prediction of oceanographic parametres in the Indian Ocean for a variety of applications, the Indian National Centre for Ocean Information Services (INCOIS) has recently set-up an operational ocean forecast system, viz. the Indian Ocean Forecast System (INDOFOS). This fully automated system, based on a state-of-the-art ocean general circulation model issues six-hourly forecasts of the sea-surface temperature, surface currents and depths of the mixed layer and the thermocline up to five-days of lead time. A brief account of INDOFOS and a statistical validation of the forecasts of these parametres using *in situ* and remote sensing data are presented in this article. The accuracy of the sea-surface temperature forecasts by the system is high in the Bay of Bengal and the Arabian Sea, whereas it is moderate in the equatorial Indian Ocean. On the other hand, the accuracy of the depth of the thermocline and the isothermal layers and surface current forecasts are higher near the equatorial region, while it is relatively lower in the Bay of Bengal.

Keywords: General circulation model, Indian Ocean variability, ocean forecast system, sea-surface temperature.

Introduction

INDIA has a long coastline extending well over 7000 km and an Exclusive Economic Zone covering 2,305,143 sq. km. About one-fourth of the country's population lives in the coastal regions. A large fraction of this population directly or indirectly depends on the surrounding ocean for a wide spectrum of activities and resources, such as traditional fishing, high-tech offshore industries, ports and harbours, shipping and tourism. Maritime security and the safety of those who venture into the sea as well as the protection of the marine environment demand accurate information and predictions of the state of the ocean in different spatial and temporal scales. The parametres on which information is required depend on the type of the activity concerned. For example, while traditional fishermen are more interested in the prediction of the sea-state and surface currents, modern fishing liners which operate in deeper waters require predictions of additional parametres such as sea-surface temperature (SST), the depth of the mixed layer and the depth of the thermocline for their cost-effective operations. Naval exercises require predictions of wave characteristics, currents and the thermohaline structure of the ocean. The activities of coast guards, such as search and rescue operations, oil-spill monitoring, etc. require forecasts of surface currents, particularly their direction and the sea-state. While ports and harbours are interested in tide predictions, the most important requirement of the shipping industry is forecast of surface currents and sea-states along the ship routes. Similarly, the offshore oil and gas industry requires accurate prediction of the thermohaline structure and the structure of currents at all levels in the water column for safe and cost-effective operations. In order to meet these various requirements, it is important to have an operational ocean forecast system based on state-of-the-art ocean general circulation models (GCMs), which are capable of simulating and predicting the dynamic and thermodynamic structure of the ocean in different space and timescales.

Several operational ocean forecast systems exist worldwide and each of them is unique because the type of ocean model used and its configuration, data assimilation schemes used to minimize the error in initial conditions, datasets assimilated into the system, atmospheric data used to force the models, etc. vary from one ocean forecast system to the other. For example, the Bluelink ocean forecast system of Australia[1] uses the modular ocean model (MOM4p0d)[2] for both the global and regional forecasts. The horizontal resolution of the regional forecasting system for Australian waters is 0.1°. The operational ocean forecast system of the United Kingdom, FOAM[3], and the Mercator Ocean[4], the forecast system of France, use the NEMO ocean model at a horizontal resolution of 0.083°. Both Bluelink and Mercator use ensemble-based assimilation schemes – Bluelink uses Ensemble Optimal Interpolation (EnOI)[5,6] and Mercator uses a variant of the Singular Extended Evolutive Kalman (SEEK)[7] filter. Different versions of the HYCOM model are extensively used in operational ocean forecasts in different parts of the world. Examples are the US-HYCOM[8] and TOPAZ, the forecast system of Norway[9] (www.topaz.nersc.no). The MIT ocean general circulation model is used in the Estimating the Circulation and Climate of the Ocean (ECCO) program[10] (www.ecco-group.org).

*For correspondence. (e-mail: shenoi@incois.gov.in)

The essential components of any operation ocean forecast system are: (a) an Ocean General Circulation Model (OGCM), (b) an appropriate data assimilation scheme to minimize error in initial conditions, (c) atmospheric forcing and (d) a set of software tools to pre-process all the input data, integrate various components of the forecast system and post-process the forecasts for the final dissemination. The quality of the forecast depends on the performance of the OGCM used, choice of the data assimilation scheme and the availability of observational data that are assimilated into the system. Since the most critical component of any forecasting system is the OGCM, choosing the right horizontal and vertical resolutions, mixing parameterization schemes and their coefficients, boundary forcing, etc. are important as they determine the quality of the simulations by an OGCM. It is often difficult to have a unique combination of these factors that performs equally well for all regions in the world's ocean. Hence, different forecasting systems have varying skills in simulating/predicting different ocean parametres and thus justify the existence of several operational ocean forecasts worldwide. Oke *et al.*[11] critically evaluated the skills of four different operational ocean forecast systems, viz. Bluelink, Mercator, US-HYCOM and FOAM, in simulating different ocean parametres in the Tasman and Coral Seas off eastern Australia. They concluded that for these regions, the Bluelink system generally performs the best for sea-level anomaly, the Mercator system for near-surface velocity, the US-HYCOM system for SST, and FOAM for sub-surface temperature and salinity, suggesting that each system has its own strengths and weaknesses.

Realizing the need for an ocean forecasting system for the Indian Ocean in general and the seas around India in particular, the Indian National Centre for Ocean Information Services (INCOIS), Hyderabad, an autonomous institute under the Ministry of Earth Science (MoES), Government of India (GoI), has recently set-up an operational ocean forecast system – the Indian Ocean Forecast System (INDOFOS) aimed at providing short-term ocean forecasts for the user community in India. The impetus to undertake this task was provided by the remarkable performance of basin-scale models of the Indian Ocean in simulating the seasonal cycle[12] as well as interannual[13] and intraseasonal[14] variations, and the launching of several observational programmes to collect data routinely from different parts of the Indian Ocean[15]. An experimental INDOFOS was set-up in January 2010 and it was upgraded in February 2012. Currently, INDOFOS provides six-hourly forecasts of four parametres, viz. SST, depths of the mixed layer (MLD) and 20°C isotherm (D_{20}, as a measure of the depth of the thermocline) and surface currents with lead time up to five days (www.incois.gov.in/Incois/indofos_main.jsp).

Indian Ocean Forecast System set-up

The OGCM, the Regional Ocean Modeling System (ROMS) – version 3.3, developed by Rutgers University, New Jersey, USA, has been used to set-up INDOFOS. In ROMS, primitive equations governing ocean dynamics and thermodynamics are discretized onto an Arakawa C-grid to obtain numerical solutions[16,17]. ROMS uses orthogonal curvilinear coordinates in the horizontal and stretched terrain following sigma coordinates in the vertical[16,18]. ROMS is one of the most widely used ocean models for operational and experimental ocean forecasts in many parts of the world. Chesapeake Bay Operational Forecast System (CBOFS, http://tidesandcurrents.noaa.gov/ofs/cbofs/cbofs.html), MED-ROMS Forecasting System for the Mediterranean Sea (http://www.med-roms.org/), South Atlantic Bight and Gulf of Mexico Circulation Nowcast/Forecast (SABGOM N/F) Modeling System (http://omglnx6.meas.ncsu.edu), Monterey Bay ROMS real-time forecasting (http://ourocean.jpl.nasa.gov/MB06), West Florida Shelf Model (WFS ROMS, http://ocgmod1.marine.usf.edu/WFS/), Experimental ocean forecast around new Caledonia (http://www.ird.nc/UR65/Marchesiello/roms_forecast_nc.html), etc. are some of the ocean forecast systems developed based on different versions of ROMS. In most of these forecast systems, the initial conditions for the forecasts are either generated by assimilating data from observation systems into the same model set-up or taken directly from other ocean analysis systems. However, at present no scheme to assimilate observations into the model is incorporated in the INDOFOS set-up. Hence, for making forecasts, INDOFOS uses the initial conditions from the simulations of the Indian Ocean set-up of the ROMS itself.

The domain of the Indian Ocean model based on ROMS extends from 30°E to 120°E in the east-west direction and from 30°S to 30°N in the north-south direction (Figure 1). The horizontal resolution of the Indian Ocean model for INDOFOS is 0.125° (approximately 13 km) and it has 40 sigma levels in the vertical. The vertical stretching parametres are chosen in such a way that the vertical resolution is highest in the upper part of the ocean. In the deep ocean (with depth more than 3500 m), there are approximately 26 levels in the top 200 m of the water column. The number of levels in the given depth of water column is more in the shallower regions. The lateral boundaries in the east and south are treated as open, where the tracer and momentum fields are relaxed to monthly climatological values derived[19,20] from the *World Ocean Atlas* (*WOA*), 2009. The western and northern boundaries are solid walls with no-slip conditions. The model uses the KPP mixing scheme[21] to parameterize the vertical mixing. Bi-harmonic[22] viscosity and diffusion schemes are chosen for horizontal mixing and a bulk parameterization scheme[23] is chosen for the computation of air–sea fluxes of heat. Sea surface salinity is relaxed to the monthly climatological values derived from *WOA* 2009 (refs 19, 20).

The model was spun up for a period of 10 years from the initial conditions, in which the temperature and salinity fields are prescribed from the WOA 2009 for January and all the components of momentum are set as zero (a state of rest). Then, it was forced with realistic atmospheric forcing for the period 2000–2012 to simulate 'true state of the ocean' in the interannual timescales. For the period 1 January 2000–30 June 2009, the model was forced with surface wind measurements from QuickSCAT and other atmospheric forcing parametres required to compute the air–sea fluxes (surface air temperature, surface specific humidity, net longwave radiation and net shortwave radiation) from the objectively analysed flux data (OAflux)[24]. In Figure 2, the time series of thermocline (D_{20}) simulated by the model for the period 2002–2006 is compared with the observation at 90°E, 1.5°S. This location is considered for the comparison due to the availability of data from Research Moored Array for African–Asian–Australian Monsoon Analysis and Prediction (RAMA) buoy for a longer period. It is clear that the model reproduces the observed intraseasonal and interannual variation of the thermocline with high accuracy at this location. It may be further noted that the model simulation does not show significant drift with time. From 1 July 2009 to 15 February 2012, six-hourly analysed atmospheric forcing fields obtained from the National Centre for Medium Range Weather Forecast (NCMRWF), New Delhi (http://www.ncmrwf.gov.in/t254-model/t254_des.pdf) were used to force the model. Since no data assimilation scheme is incorporated into the INDOFOS set-up, the initial conditions for the forecasts are taken from the simulations of the model itself, which is forced by the atmospheric analysis provided by NCMRWF. The atmospheric forcing to integrate the model in the forecast mode is also taken from six-hourly forecasts issued by the NCMRWF. Each atmospheric forcing dataset obtained from NCMRWF consists of forecasts for the succeeding five-days (20 time-steps). Every day after the ocean model is forced by the analysed atmospheric data to obtain the best estimate of the state of the ocean (initial condition for the forecasts), the model is forced by the atmospheric forecast data for the next five-days. At the end of each forecast cycle, it generates a six-hour averaged ocean analysis for the previous day and an ocean forecast for the next 120 h. The forecasts are then issued in text and graphical formats through the webpage http://www.incois.gov.in/Incois/indofos_main.jsp. These forecasts are freely accessible to the public. The forecast data are also made available for registered users for non-commercial applications. The entire procedure from downloading the forcing data from NCMRWF to uploading the final forecasts to the INCOIS website is automated so that manual intervention in the operations is minimal.

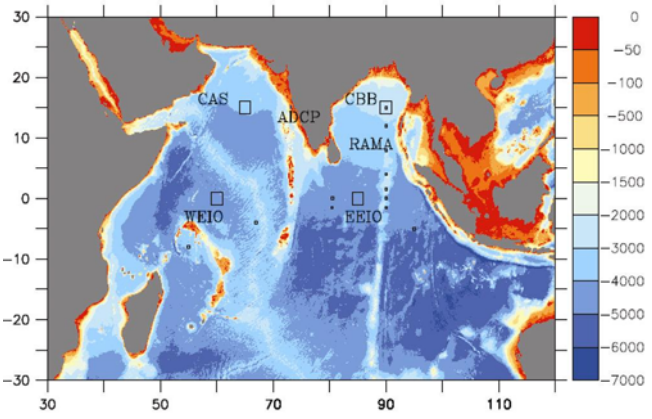

Figure 1. Map of the bathymetry (in m) used to set up ROMS. Locations selected for the validation of sea-surface temperature (SST) are shown as large black boxes. Locations of the RAMA buoys considered in this study are also shown as small black boxes. Location of coastal Acoustic Doppler Current Profiler off Goa is shown in small blue box.

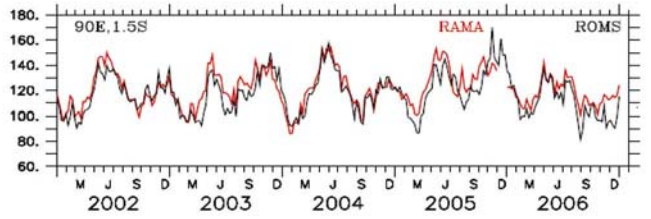

Figure 2. Time series of depth (in m) of 20°C isotherm simulated by ROMS is compared with the RAMA buoy observation at 90°E, 1.5°S for the period 2002–2006.

Data

In this study, the daily averaged operational products of INDOFOS for the period 15 February–15 November 2012 are validated using available *in situ* and remote sensing observations. SST predictions are validated using 3-day mean SST data from the Tropical Rainfall Measuring Mission (TRMM) Microwave Imager (TMI)[25,26] and data from the moored buoy array in the Indian Ocean (the RAMA moorings)[27]. Daily mean surface current and subsurface temperature observations from the RAMA moorings are used for the validation of surface currents and D_{20}. Merged sea-level anomaly data produced by AVISO (http://www.aviso.oceanobs.com/duacs) are used in this study to identify the characteristic features of circulation in the western Indian Ocean. We also use the subsurface current measurements off the coast of Goa by Acoustic Doppler Current Profiler (ADCP)[28] deployed and maintained by CSIR-National Institute of Oceanography (NIO), Goa for the period 1 November 2009–31 October 2010 to compare the coastal currents simulated by the ROMS set-up for the same period.

Validation of the forecasts

Sea-surface temperature

SST is an important parameter in operational ocean prediction. For example, the routine potential fishing zone (PFZ)

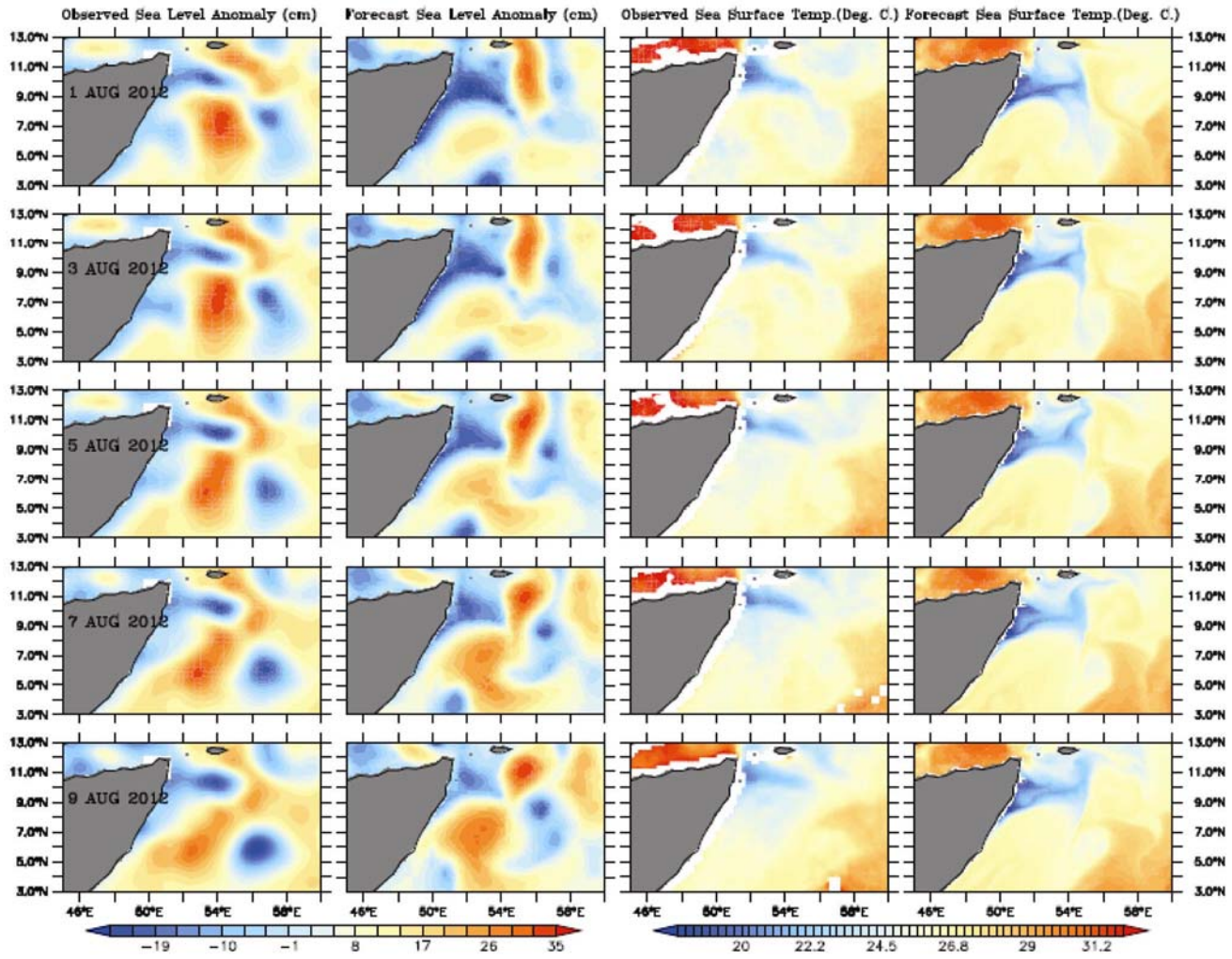

Figure 3. Sequence of observed sea-level anomaly (panels in the first column) and SST (panels in the third column) and predicted (with 3-day lead) sea-level anomaly (panels in the second column from the left) and SST (panels in the last column). Note that predicted SST faithfully captures the transformations in the Great Whirl during 1–9 August 2012.

advisories issued by INCOIS and many other agencies in the world make use of the information on the gradient in the SST field where the biological production could be high, if other ambient conditions are favourable[29–32], for identifying the regions with higher chances for fish catch. Hence the accurate prediction of SST can significantly improve the quality of PFZ advisories. SST patterns may be used to identify regions of upwelling and the circulation features associated with it. The western part of the northern Arabian Sea is one of the regions in the Indian Ocean where the biological production is significantly high due to strong upwelling during the Indian summer monsoon. The upwelling brings nutrient-rich water to the surface off the coasts of Somalia and Oman[33]. The phytoplankton blooms that are associated with this upwelling persist until September[34–36]. These phytoplankton blooms are apparent in the field observations and satellite data during the southwest monsoon period and spread well offshore of the initial upwelling regions due to the characteristic circulation features of the region. Another prominent feature of circulation in this region is an anticyclonic gyre, known as the 'Great Whirl'[37–39]. The structure of the Great Whirl can be easily identified in the maps of sea-level anomaly and SST. The observed and predicted sequences of SST and sea-level anomaly during the dissipation of such an eddy, during 1–9 August 2012 are shown in Figure 3. The predictions shown in Figure 3 are with 3-day lead time. The presence of an anticyclonic gyre and the associated advection of cooler upwelled water from the coast are clearly visible in the sea-level anomaly pattern as well as in the SST map on 1 August. Further, the decaying gyre on 9 August is also visible in the maps of sea-level anomaly and SST. It is important to note that location and evolution of this gyre are well predicted by INDOFOS (Figure 2). However, the offshore edge of the cold patch in the forecast does not match well with the observation. This may be due to the inability of the model to

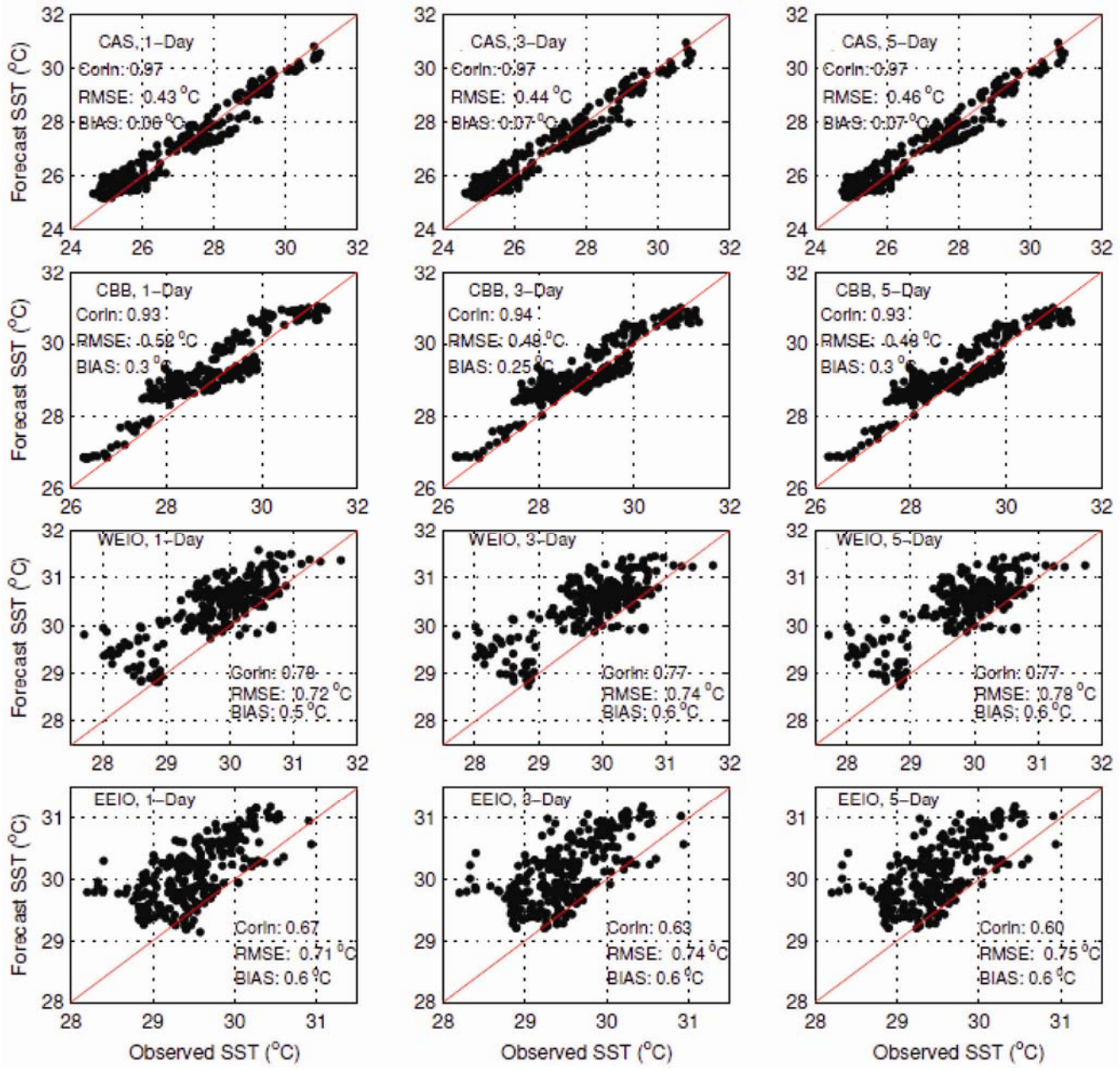

Figure 4. Predicted SST plotted against observations at the locations shown in Figure 1. (Left panels) SST forecast with a 1-day lead; (Middle panels) For 3-day lead forecasts; (Right panels) For 5-day lead forecasts.

reproduce the exact structure of the circulation pattern in this region.

In order to estimate the errors in the predicted SST quantitatively, we have selected four regions in the Indian Ocean: central Arabian Sea (CAS, 64–66°E, 14–16°N), central Bay of Bengal (CBB, 89–91°E, 14–16°N), western Equatorial Indian Ocean (WEIO, 59–61°E, 1°S–1°N) and eastern equatorial Indian Ocean (EEIO, 84–86°E, 1°S–1°N) as shown in Figure 1. Figure 4 shows the predicted SST with 1-day, 3-day and 5-day leads plotted against the TRMM Microwave Imager (TMI) SST data for these regions. It is clear that the SST predictions in the Arabian Sea (*a–c*) and Bay of Bengal (*d–f*) are in good agreement with the observations with high correlation (0.97 and 0.93 respectively) and low root mean square error (RMSE, 0.46°C, 0.48°C). However, the correlation coefficients are relatively low (0.76) and RMSE is relatively high (0.76°C) in the eastern and western equatorial Indian Ocean. In addition, there is a significant positive bias (0.5°C) in the SST predictions in the equatorial regions. It may be noted that the range of SST variability in the equatorial region is rather low compared to the central Arabian Sea and the Bay of Bengal; that could be one of the reasons for the poor skill of the predictions.

The correlation coefficients and the RMSE are comparable to those for the four major operational forecast systems for the Australian Coral Seas, which are between 0.5–0.75, and 0.5°C and 0.8°C respectively[11]. The frequency distribution of the absolute error in the SST predictions as well as its cumulative frequency (considering all the four regions shown in Figure 1) by INDOFOS is shown in Figure 5. Approximately in 80% cases, the error is less than 0.8°C and it is above 1.0°C only in less than 10% of the cases.

It may be noted that the distribution of error, correlation coefficient and RMSE do not vary significantly with forecast lead time. The reason for this consistency in the performance could be due to the absence of ocean data assimilation into the model. In the absence of data assimilation, the initial conditions used for the predictions and 'the true' state of the ocean simulated by the model remain more or less the same. Since the model has not drifted significantly from the initial condition, the short-term variation in different parametres probably arises from the variation in the atmospheric forcing. Hence the difference in the quality of predictions with lead time is essentially due to the difference in the quality of the atmospheric forcing. Prasad *et al.*[40] showed that, in general, the accuracy of the atmospheric predictions by NCMRWF is fairly good up to 3-days lead time and reasonably good up to 5-days lead time.

RAMA moored buoy observations provide long time series of *in situ* measurements of temperature, salinity and currents at different depths at several locations in the Indian Ocean. Time series of the SST predictions from INDOFOS at 90°E, 8°N; 90°E, 15°N; 90°E, EQ and 55°E, 8°S are compared with the buoy observations in Figure 6. The SST predictions are close to the observations in the Bay of Bengal, while there is a bias of approximately +0.5°C in the eastern equatorial Indian Ocean. In the southwestern Indian Ocean, the SST predictions are quite accurate till middle of May and after mid-May, the predicted SST appears to be higher than the observation by approximately 0.3°C. The predicted SST at different locations is plotted against the moored buoy observations in Figure 7. It may be noted that the accuracy of the predicted SST varies with location, and it is relatively high in the central Bay of Bengal compared to that in the equatorial Indian Ocean.

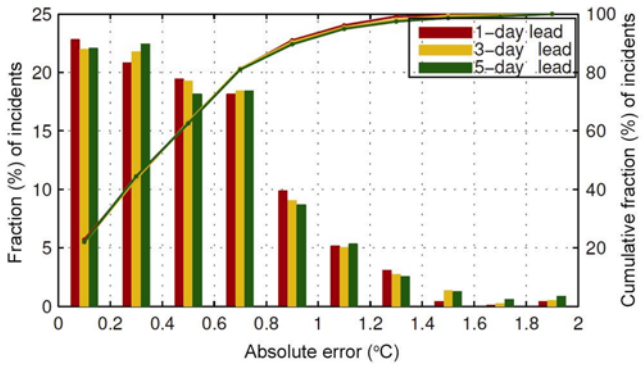

Figure 5. Frequency distribution of absolute error in SST forecasts (magnitude of the difference between the forecast and observation), with different lead times, at the locations shown in Figure 1. The cumulative frequency distributions are shown as continuous lines. The axis on the right side represents cumulative frequency distribution.

The rate of change is an important information in short-term forecasts as it essentially indicates whether the SST tends to increase or decrease on daily timescales. Predicted rate of change of SST (by constructing time series of all the 3-day lead predictions) is compared with the rate observed by the RAMA moorings in Figure 8. It may be seen that on most of the occasions, the phase and magnitude of the SST changes are predicted realistically by INDOFOS. The daily fluctuations in SST with larger magnitude in the southwestern Indian Ocean are also predicted realistically by the system. Statistical evaluation of the predicted SST with respect to the RAMA buoy observations is given in Table 1. It may be noted that the root mean square error of SST forecasts is much less than the natural variability (standard deviation) for locations away from the equator. However, the quality of predictions is not good near the equator.

Surface current

Predictions of surface currents are critical for a wide range of applications such as search-and-rescue operations, estimation of optimal ship routes, prediction of oil-spill trajectories, traditional and high-tech fishing activities, etc. Yet, the accuracy of the predictions of surface currents is relatively low in almost all operational forecasting systems due to several reasons. For example, the estimated RMSE in surface current predictions for the East Australian waters by the four leading operational ocean prediction systems are of the order of 25–40 cm s^{-1} and the correlation coefficients between the observed and predicted surface current components in this region are also relatively low (in the range 0.2–0.7)[11].

The zonal (u) and meridional (v) components of surface currents predicted by INDOFOS (with 3-day lead time) and their daily rate of change at three locations along 90°E (equator, 4°N and 8°N) where there are continuous data available of surface currents from the RAMA moored buoy are compared with observations in Figures 9 and 10 respectively. The statistics of the validation (viz. the correlation coefficients, standard deviation of both observations as well as the predictions and RMSEs) are given in Table 2 for the zonal component and in Table 3 for the meridional component. The predictions match fairly well with the observations for both the components of the surface current at the equator. The RMSEs are 22 and 24 cm s^{-1} and the correlation coefficients are 0.75 and 0.45 for the u and v components respectively. At 4°N, the correlation coefficients between the observation and the predictions dropped to 0.4 (for

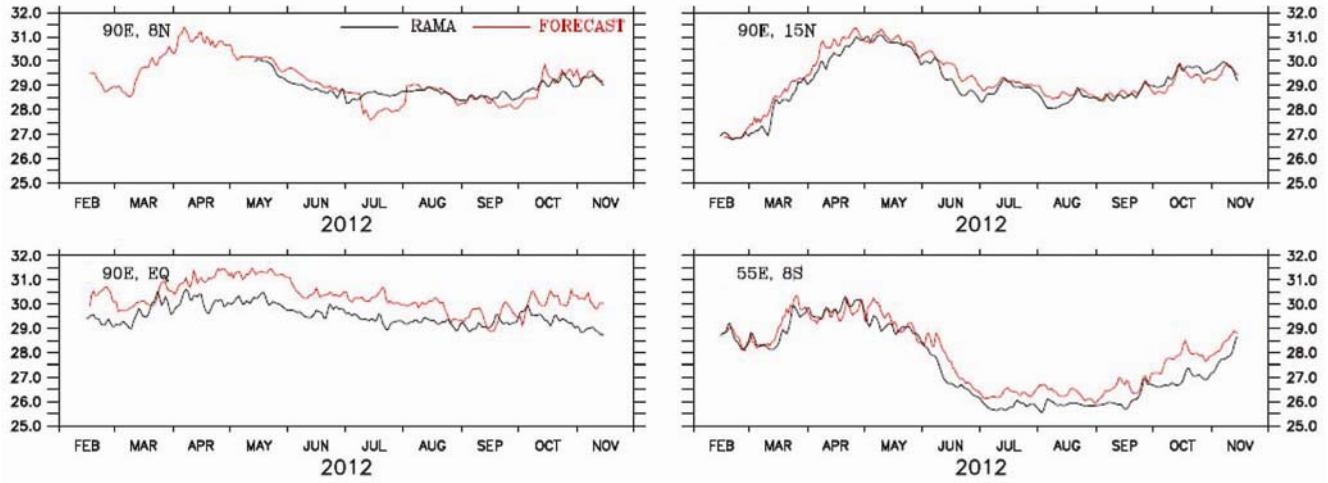

Figure 6. Time series of observed (RAMA buoy) and predicted SST (°C) at four locations in the Indian Ocean.

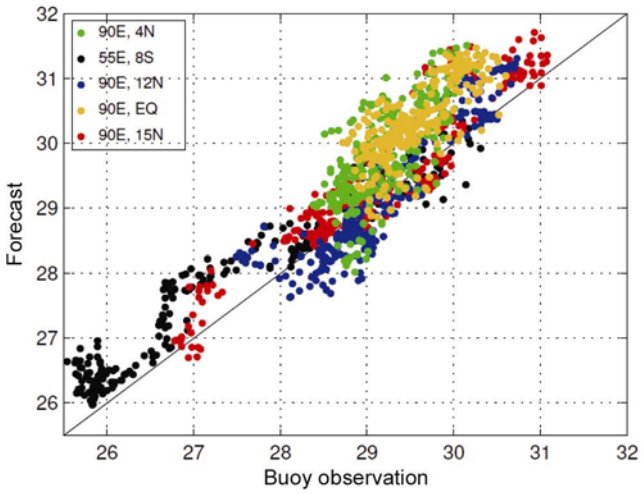

Figure 7. SST (°C) predicted by INDOFOS plotted against the observations (RAMA buoys) at selected locations in the Indian Ocean. Dots with different colours represent data from different locations.

both the components) with RMSE slightly higher than the standard deviations. It may be noted that the quality of the prediction of the surface current decreases away from the equator. The comparison between the observed and predicted values of both *u* and *v* are particularly poor at 90°E, 8°N (Figure 9). At this location the RMSEs are higher (41 and 29 cm s^{-1} respectively, for *u* and *v*) and correlation coefficients are poor (almost 0 for both the components). This is intriguing and it requires detailed studies to understand this gross mismatch between the observation and the forecast.

Figure 11 shows the scatter plots of predicted versus observed components of surface currents from RAMA moorings at several locations (90°E, EQ; 90°E, 4°N; 90°E, 8°N; 80.5°E, EQ and 55°E, 8°S) where data are available for the period during 15 February–15 November 2012. At 80.5°E, EQ and 55°E, 8°S, continuous data are not available. The combined RMSEs are 28 and 25 cm/s (for the *u* and *v* components respectively) and correlation coefficients are 0.6 and 0.44 (for the *u* and *v* components respectively). Notably, these values are comparable to those reported by Oke *et al.*[11] for the predictions in East Australian coastal waters. However, further analysis involving validation of the forecasts from different systems for a given location is needed to compare the performance of the forecasting systems.

Depth of the thermocline

Most of the heat in the ocean is stored in the water column above the thermocline. The depth of the 20°C isotherm (D_{20}) is generally considered as a measure of the depth of the thermocline in the tropics[41]. Variation in the thermocline is an important indicator of the internal processes within the ocean due to ocean dynamics. The thermocline tends to be deeper in regions where upper-layer currents converge and shallow where they diverge. Hence the accurate representation of this variation in thermocline depth points to the quality of simulations by OGCMs. The depth of the thermocline varies from a few tens of metres to a few hundreds of metres in the tropical oceans. Though the fluctuations in the depth of thermocline are of the order of few metres per day, a larger variability in the tropics is generally associated with seasonal or annual cycles driven by large-scale ocean dynamics.

The daily variations of predicted (with 3-day lead) D_{20} at six different locations in the eastern equatorial Indian Ocean and the Bay of Bengal are compared with the RAMA moored buoy observations in Figure 12. Detailed statistics of the validation is given in Table 4. The predicted and observed depths of the thermocline match well at 90°E, 5°S; 90°E, 1.5°S and 90°E, 4°N. But prediction of the thermocline is not so good in the Bay of Bengal

Table 1. Standard deviation of observed and predicted sea-surface temperature (SST) at selected locations where RAMA moored buoy data are available. Root mean square error of the prediction and the correlation coefficient between the observed and predicted SST at these locations are also given

	90°E, 15°N	90°E, 12°N	90°E, 4°N	90°E, EQ	55°E, 8°S
Standard deviation (OBS; in °C)	1.1	0.75	0.5	0.42	1.4
Standard deviation (ROMS; in °C)	1.1	0.95	0.8	0.56	1.3
RMSE (in °C)	0.46	0.42	0.8	0.8	0.54
Correlation coefficient	0.94	0.9	0.75	0.75	0.96

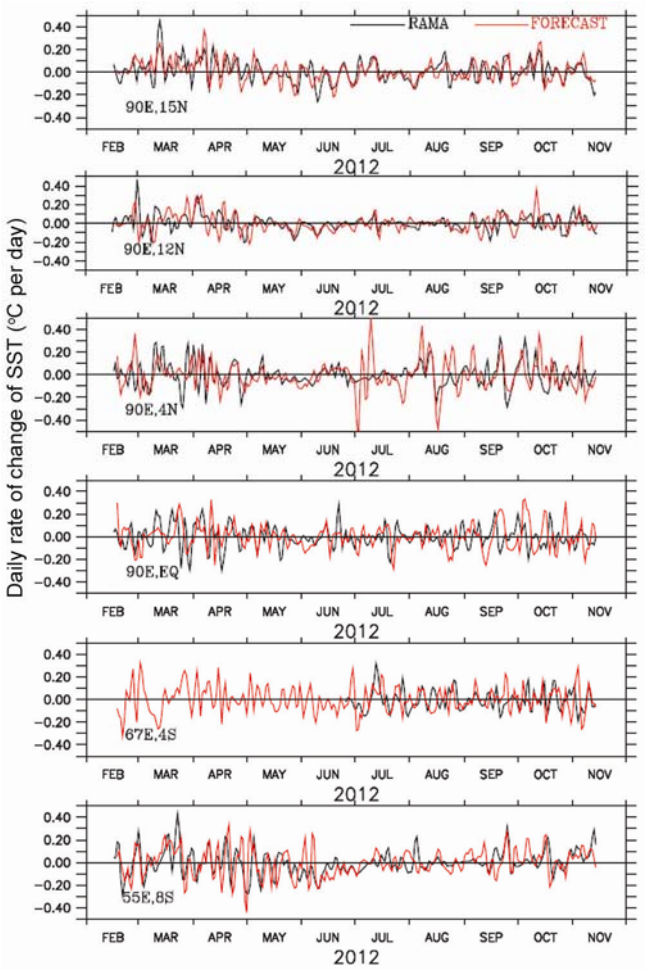

Figure 8. Rate of change of SST (°C day^{-1}) with time as predicted by INDOFOS (with 3-day lead time) and that observed by the RAMA buoys.

(at 90°E, 8°N; 90°E,12°N and 90°E, 15°N). This indicates that the model is better equipped to capture the thermocline at lower latitudes and not so for the higher latitudes. Accordingly, the correlation coefficients also decrease from 0.9 (at 95°E, 5°S) to 0.3 (90°E, 15°N). This is consistent with the poor performance of the system to predict surface currents in the Bay of Bengal. For most of the locations, the RMSEs of the thermocline predictions are less than 13.0 m, except at 90°E, 12°N, where it is significantly higher (21.0 m). This high RMSE is due to the gross overestimation of the thermocline depth, particularly during the summer monsoon months, compared to actual observations. The overall correlation between the observed and predicted D_{20} is 0.6 and the RMSE is 13.0 m. This is quite remarkable given the fact that no data are assimilated to the prediction system. The frequency distribution of the absolute error of the D_{20} estimate is shown in Figure 13. It may be noted that in more than 60% of the cases, the difference between the observed and predicted D_{20} is less than 10.0 m and only in 10% of the cases it is greater than 25.0 m.

The depth of the isothermal layers

The surface mixed layer in the ocean is the layer in which the physical properties of the water such as temperature, salinity (and hence density), etc. do not vary considerably with depth due to turbulent mixing processes. Being the interface between the atmosphere above and the ocean beneath, the mixed layer plays an important role in air–sea interaction processes. Momentum from winds and the air–sea fluxes are directly distributed within the mixed layer at first. Hence, an accurate representation of mixed layer is critical for good simulations of parametres such as SST, surface currents, etc. by numerical models. There are several criteria for defining the mixed layer depth (MLD)[42,43] and one among them is the depth at which the density of sea water is higher by 0.125 kg m^{-3} than the density at the surface[44]. Predictions by INDOFOS also use this criterion to define MLD. However, due to the non-availability of continuous observed salinity data, which are required to compute the density of sea water, we have redefined the MLD in this article as the depth at which the temperature is less than the SST by 0.5°C, which is also a commonly used definition for the MLD[45–47]. This is also referred to as the isothermal layer depth (ILD). A comparison of the MLD and ILD computed using the INDOFOS forecast data for four selected locations in the Indian Ocean is shown in Figure 14. It may be noted that near the equator, the MLD and ILD do not differ much. However, away from the equator, the differences are very large.

The daily variation of the predicted (with 3-day lead time) ILD at four locations in the Indian Ocean (90°E, 15°N; 90°E, 4°N; 90°E, EQ and 55°E, 8°S) is plotted

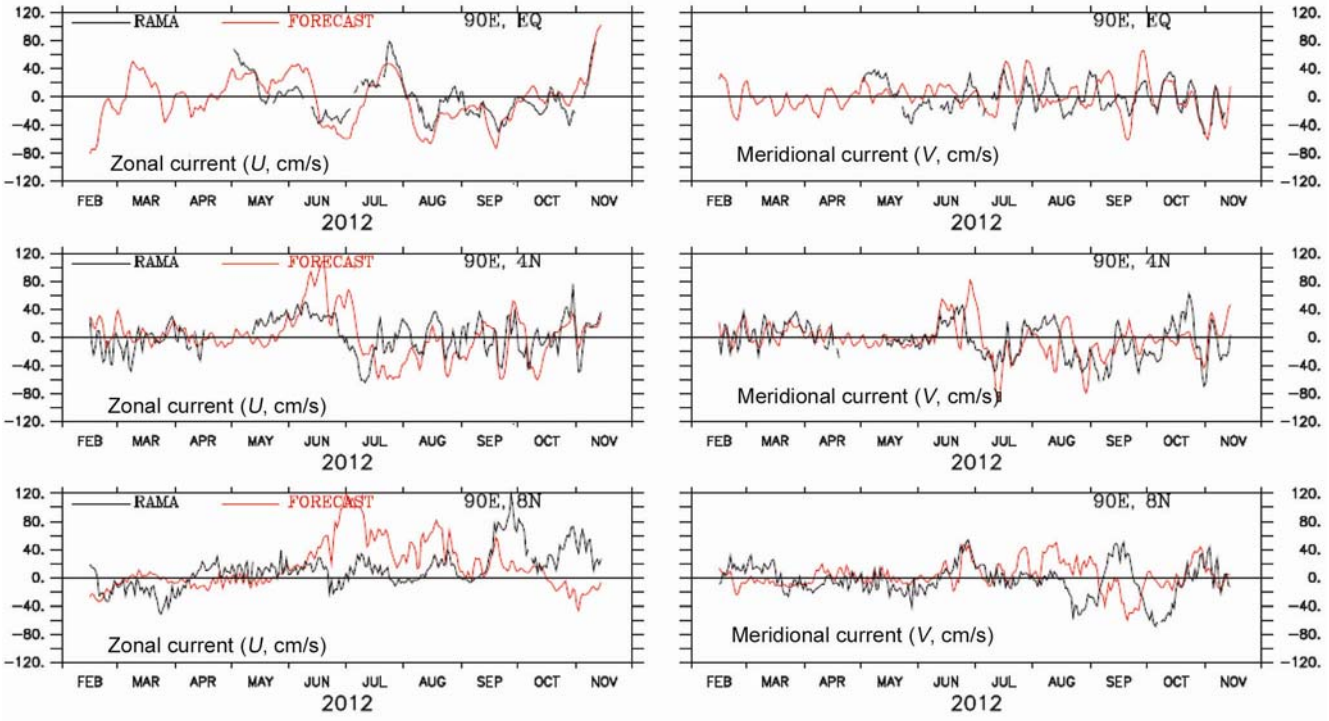

Figure 9. Variation of the observed (from RAMA buoys) and predicted zonal component of the surface current (left panels) and meridional current (right panels) along 90°E at the equator, 4°N and 8°N.

Table 2. Same as Table 1, but for zonal component of the surface currents

	90°E, 8°N	90°E, 4°N	90°E, EQ
Standard deviation (OBS; in cm s^{-1})	27	25	28
Standard deviation (ROMS; in cm s^{-1})	33	33	33
RMSE (in cm s^{-1})	42	32	22.0
Correlation coefficient	0.04	0.4	0.75

Table 3. Same as Table 1, but for meridional component of the surface currents

	90°E, 8°N	90°E, 4°N	90°E, EQ
Standard deviation (OBS; in cm s^{-1})	23	25	21
Standard deviation (ROMS; in cm s^{-1})	18	25	22
RMSE (in cm s^{-1})	29	27	24.0
Correlation coefficient	0.07	0.4	0.45

along with observations in Figure 15 and its daily rate of change is shown in Figure 16. It may be seen that the variability of the ILD at high frequency near the equatorial ocean is predicted well by the system. However, the skill of the forecast system to predict high-frequency variations away from the equator is not satisfactory. Nevertheless, it succeeded in capturing the seasonal cycle of ILD realistically. In general, the predicted ILD is deeper than the observed. In addition, the predicted magnitudes of large changes in ILD do not agree well with the observations. This deficiency of the model is more prominent in the Bay of Bengal than in the equatorial Indian Ocean. The observed standard deviation of the ILD at the four locations given above is 23.0 m, while it is only 16.0 m in the predictions. The correlation between the predicted and observed ILD, however, is quite high (0.74). This may be attributed to the skill of the model to simulate the seasonal cycle realistically. A detailed statistics of the comparison between the observed and predicted ILD is given in Table 5. In all the locations, even though the RMSE of the ILD prediction is much less than the observed natural variability (standard deviation), there is a necessity for substantial improvements in the quality of predictions. The distribution of absolute error in the ILD

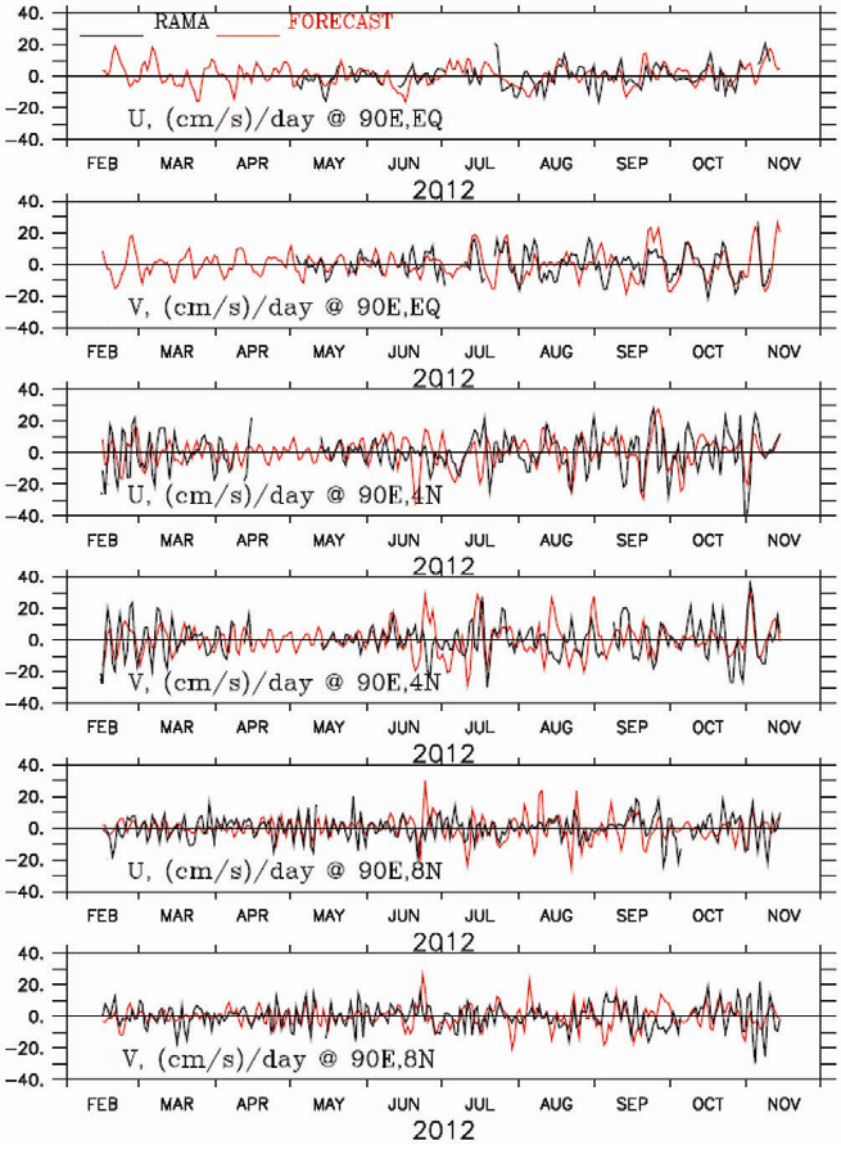

Figure 10. Rate of change (in (cm s^{-1}) day^{-1}) of the observed (RAMA buoys) and predicted surface zonal currents and meridional currents at selected latitudes along 90°E.

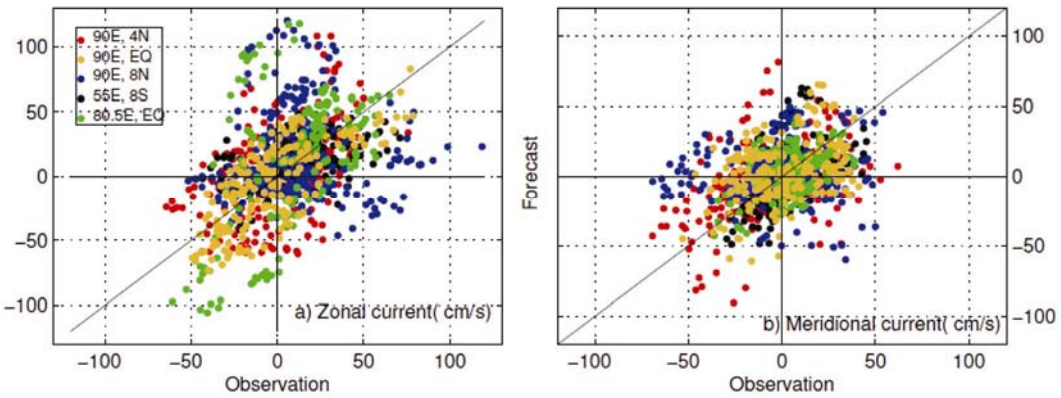

Figure 11. Scatter plots of surface current components – observed versus predicted. All available observations from RAMA buoys at 90°E, EQ; 90°E, 4°N; 90°E, 8°N; 80.5°E, EQ and 55°E, 8°S for the period 15 February–15 November 2012 are used here.

Table 4. Same as Table 1, but for the depth of 20°C isotherm

	90°E, 15°N	90°E, 12°N	90°E, 8°N	90°E, 4°N	90°E, 1.5°N	90°E, 5°S
Standard deviation (OBS; in m)	10	7	9	14	13	16
Standard deviation (ROMS; in m)	8	16	11	17	10	13
RMSE (in m)	11	21	13	12	12.3	7
Correlation coefficient	0.33	0.52	0.57	0.72	0.70	0.91

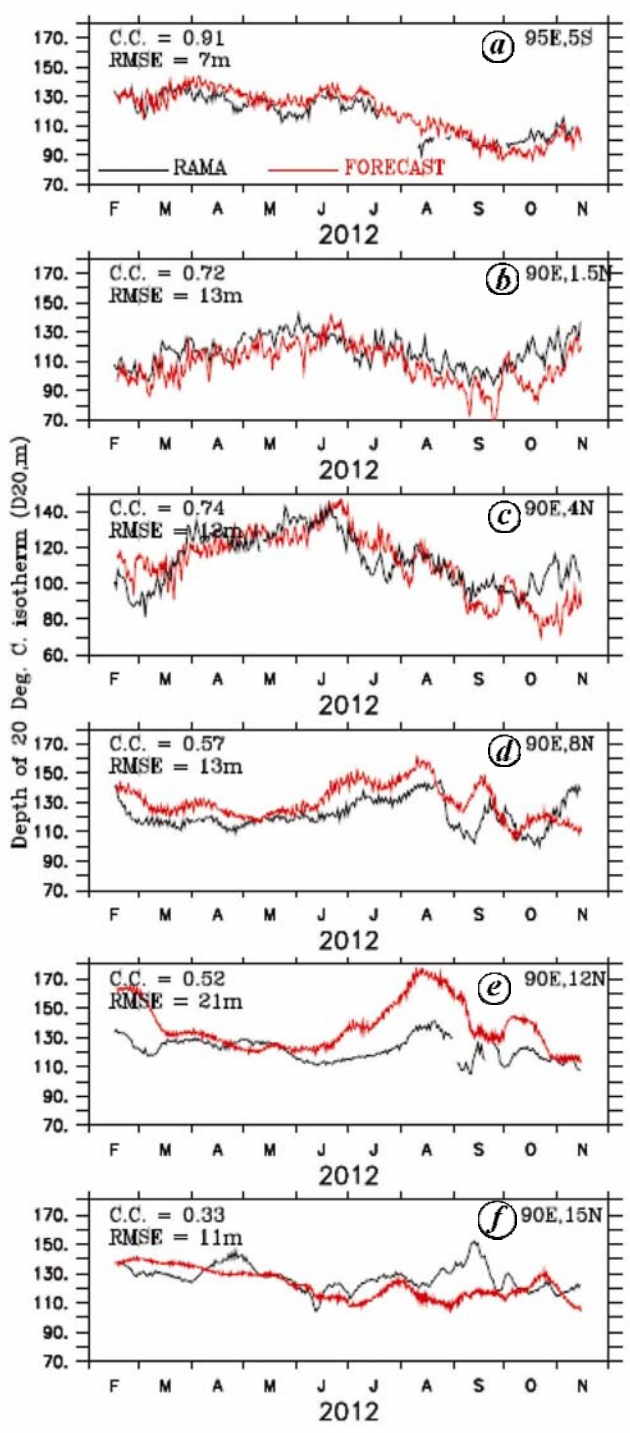

Figure 12. Time series of predicted and observed D_{20} at (***a***) 95°E, 5°S; (***b***) 90°E, 1.5°N; (***c***) 90°E, 4°N; (***d***) 90°E, 8°N; (***e***) 90°E, 12°N and (***f***) 90°E, 15°N.

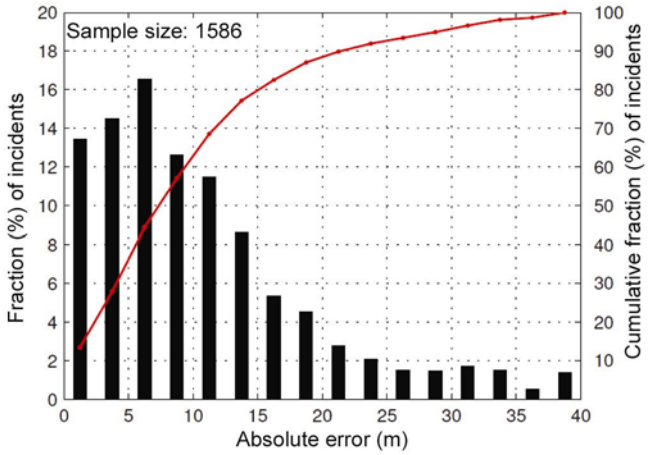

Figure 13. Frequency distribution of the absolute error in the D_{20} forecasts during 15 February–15 November 2012 at RAMA buoy locations considered in Figure 11. The cumulative frequency distribution is shown as continuous lines. The axis on the right represents cumulative frequency distribution.

(shown in Figure 17) suggests that in more than 50% of the cases the error is less than 10.0 m and larger differences (higher than 20.0 m) occur only in 20% of the cases.

Way forward

The present set-up of INDOFOS is the first attempt of its kind in the country that makes use of an OGCM to predict oceanographic parametres in short timescales. The system received an overwhelming response from the user community, including the Indian Navy and Coast Guard. The forecasts are routinely used by fishermen as well, and they receive it in their local languages. As the demand for ocean forecasts increases from the wide spectrum of users, it is important to improve the quality of the predictions. One of the drawbacks of the present forecast system is that due to the numerical constraints arising from the lower resolution of the model, the depth of the sea floor is increased to 75 m, if it is less than the same. Hence, the present set-up of the model may not be ideal for regions close to the coast. The time–depth section of the alongshore component of currents off Goa (72.7°E, 15.1°N) simulated by ROMS for the period 4 January 2010–31 October 2010 is shown together with observations from an ADCP for the same period in Figure 18. One obvious mismatch between the observation simulation

Table 5. Same as Table 1, but for the depth of isothermal layer

	55°E, 8°S	90°E, 15°N	90°E, 4°N	90°E, EQ
Standard deviation (OBS; in m)	14	22	19	18
Standard deviation (ROMS; in m)	13	17	14	15
RMSE (in m)	12.5	14	18	17
Correlation coefficient	0.80	0.80	0.5	0.72

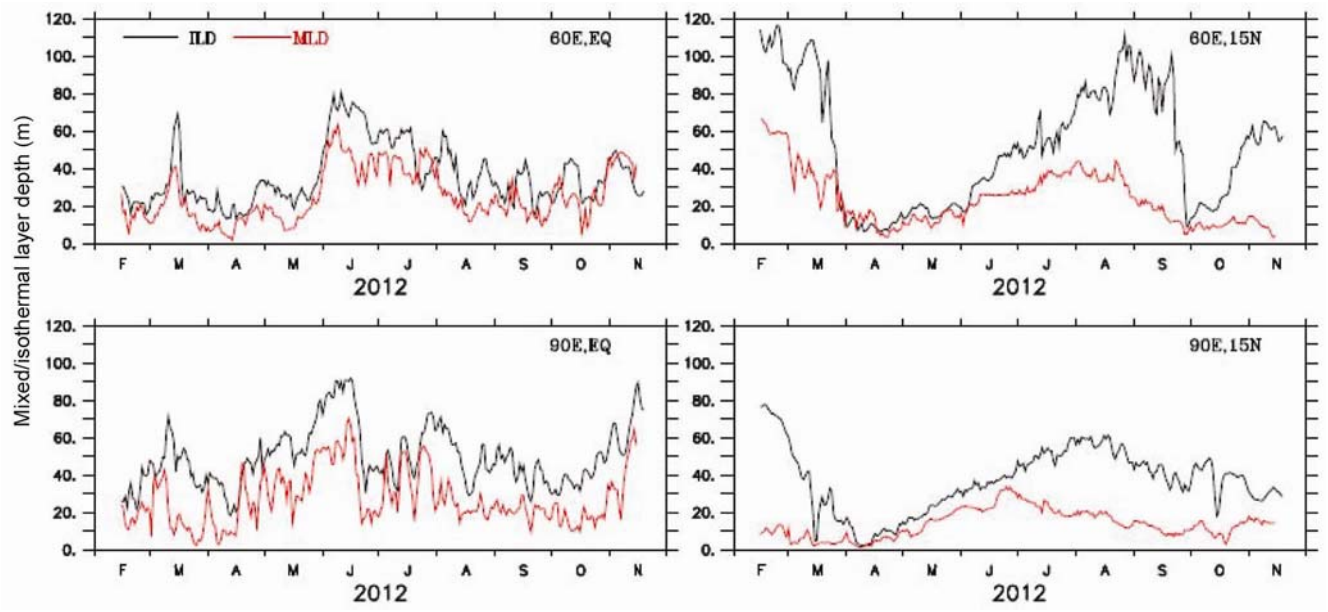

Figure 14. The mixed layer depth (in m) at four selected locations in the Indian Ocean derived using 0.25 kg m^{-3} density criteria compared with isothermal layer depths derived using 0.5°C temperature criteria at the same locations.

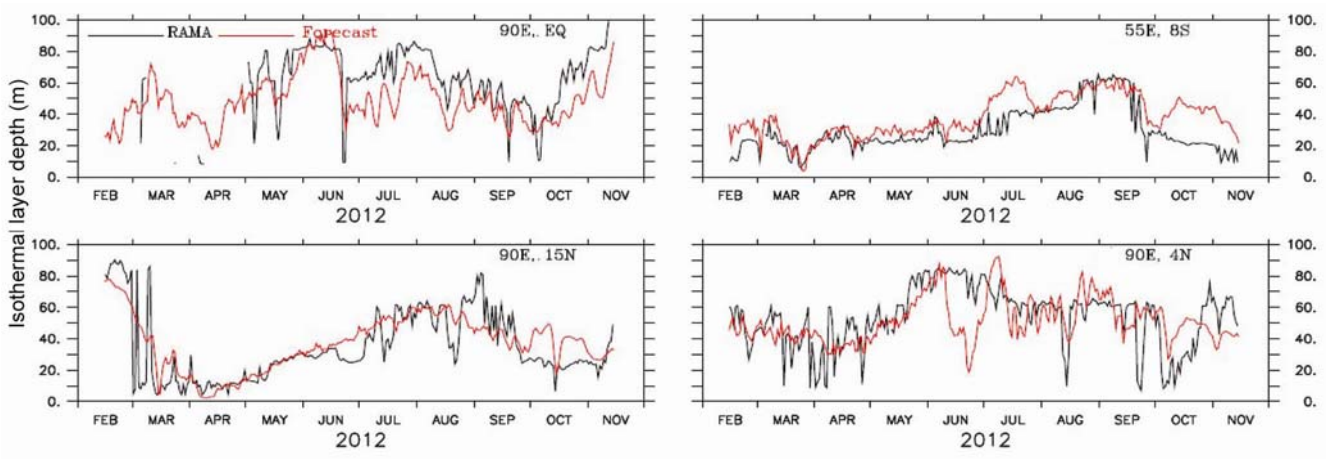

Figure 15. The daily time series of the isothermal layer depth (ILD, in m) predicted by INDOFOS compared with ILD (in m) derived using observations from RAMA moored buoys at selected locations.

is during February and March 2010, when the model did not simulate the commencement of the observed equatorward flow realistically. Further, during the southwest monsoon, the equatorward current extended to deeper levels in the simulation compared to the observation. Clearly, improvements in the model set-up, either its resolution, physics or forcing, are necessary to improve the forecast. Further, while most operational ocean forecast systems have incorporated appropriate data assimilation schemes to reduce errors in initial conditions, no such scheme has been incorporated into INDOFOS yet. Hence, it is planned to improve the operational forecast

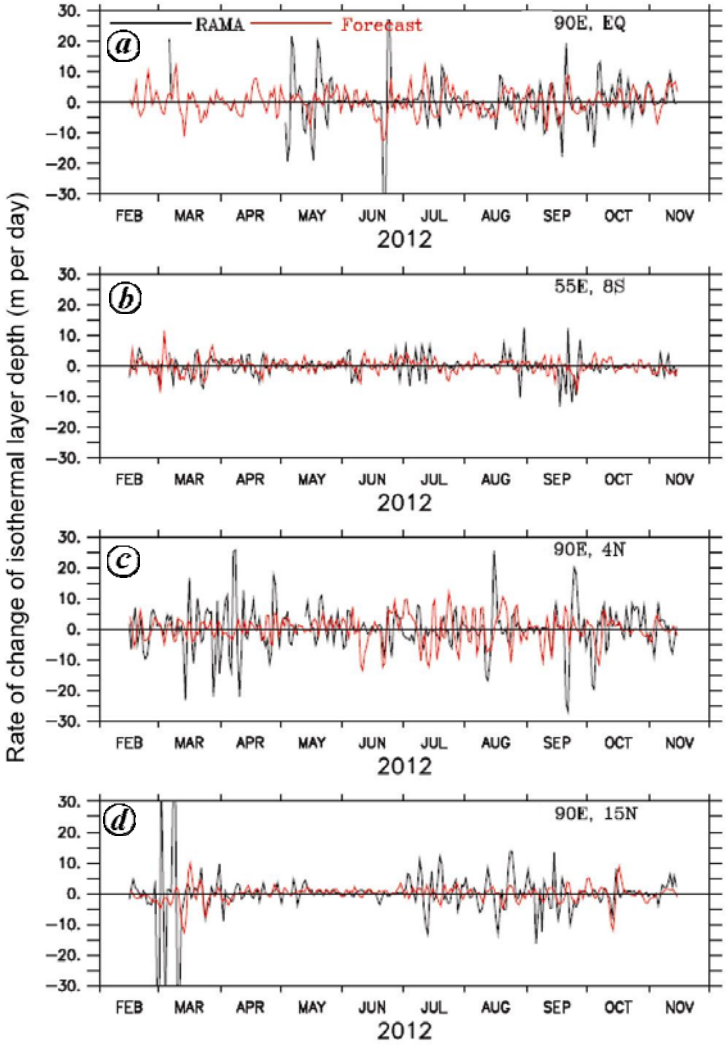

Figure 16. Daily rate of change in the predicted ILD (in m day^{-1}) compared with the observations from RAMA moored buoys at (***a***) 90°E, EQ; (***b***) 55°E, 8°S; (***c***) 90°E, 4°N and (***d***) 90°E, 15°N.

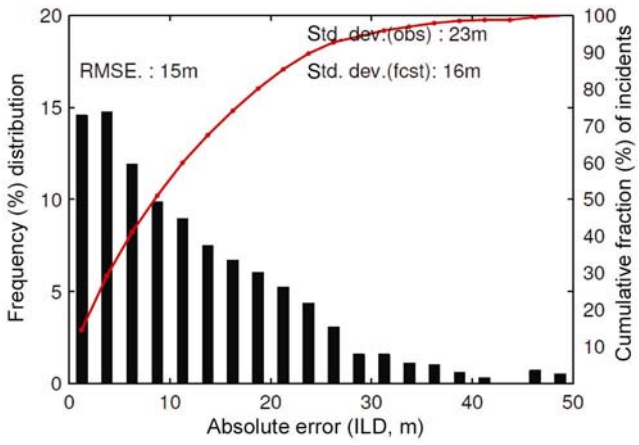

Figure 17. Frequency distribution of absolute error in the ILD forecasts during 15 February–15 November 2012 at RAMA buoy locations considered in Figure 15. The cumulative frequency distribution is shown as continuous lines. The axis on the right represents cumulative frequency distribution.

system, in which a hierarchy of models will be used at varying horizontal resolutions (ROMS with approximately 1.5 km resolution near the Indian coasts, HyCOM with approximately 9 km resolution in the Indian Ocean and MOM4p0d with about 25 km resolution outside the Indian Ocean), mixing parameterization schemes and processes such as tides and waves. Appropriate data assimilation schemes will also be incorporated in the proposed multi-model High resolution Operational Ocean Forecast and re-analysis System (HOOFS).

Summary

A description of the INDOFOS and forecasting procedures and evaluations of issued forecast variables are presented in this article. Predictions of SST, surface currents, MLD and depth of the thermocline by INDOFOS are validated using the *in situ* and remote sensing observations. The error in the SST prediction is quite low (~ 0.3–

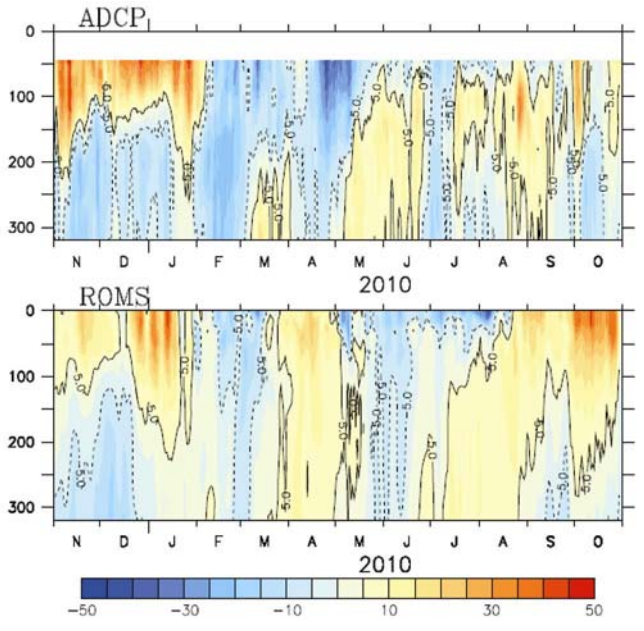

Figure 18. The time–depth section of the alongshore component of current (cm s^{-1}) off Goa (72.7°E, 15.1°N) simulated by ROMS (lower panel) for the period 1 November 2009–31 October 2010 compared with the observation from an acoustic Doppler current profiler (ADCP, upper panel).

0.45°C) and the correlation between the observation and prediction is very high (above 0.9) in the Arabian Sea and the Bay of Bengal. The accuracy of SST predictions in the equatorial Indian Ocean is relatively low with a correlation coefficient of 0.7 and an RMSE of 0.75°C. When compared with the RAMA moored buoy observations, the surface current predictions are fairly accurate in almost all the locations, except 90°E, 8°N. While the RMSE of the zonal and meridional components of surface current prediction is less than 25 cm s^{-1} at most of the locations, it is as high as 41 and 30 cm s^{-1} respectively at 90°E, 8°N. The prediction of variations in the thermocline depth near the equatorial region is quite accurate, while that in the Bay of Bengal is less accurate. The shorter timescale variations in isothermal layer depths are predicted by INDOFOS realistically, but the magnitudes of this variation are underestimated. Given the fact that no data are assimilated into this prediction system to correct the error in the initial conditions, the results are quite encouraging. It is expected that future forecasting systems with improved model physics, parameterization and grids, and the incorporation of an appropriate data assimilation scheme will improve the forecast significantly.

1. Oke, P. R., Schiller, A., Griffin, G. A. and Brassington, G. B., Ensemble data assimilation for an eddy-resolving ocean model. *Q. J. R. Meteorol. Soc.*, 2005, **131**, 3301–3311.
2. Griffies, S. M., Pacanowski, R. C. and Rosati, A., A technical guide to MOM4. GFDL Ocean Group Technical Report No. 5 NOAA/Geophysical Fluid Dynamics Laboratory, 2004, p. 371.
3. Martin, M. J., Hines, A. and Bell, M. J., Data assimilation in the FOAM operational short-range ocean forecasting system: a description of the scheme and its impact. *Q. J. R. Meteorol. Soc.*, 2007, **133**, 981–995.
4. Brasseur, P. *et al.*, Data assimilation for marine monitoring and prediction: the Mercator operational assimilation systems and the MERSEA developments. *Q. J. R. Meteorol. Soc.*, 2005, **131**, 3561–3582.
5. Oke, P. R., Allen, J. S., Miller, R. N., Egbert, G. D. and Kosro, P. M., Assimilation of surface velocity data into a primitive equation coastal ocean model. *J. Geophys. Res. C*, 2002, **107**, 3122–3147.
6. Evensen, G., The ensemble Kalman filter: theoretical formulation and practical implementation. *Ocean Dyn.*, 2003, **53**, 343–367.
7. Testut, C. E., Brasseur, P., Brankart, J. M. and Verron, J., Assimilation of sea-surface temperature and altimetric observations during 1992–1993 into an eddy permitting primitive equation model of the North Atlantic Ocean. *J. Mar. Syst.*, 2003, **40–41**, 291–316.
8. Cummings, J. A., Operational multivariate ocean data assimilation. *Q. J. Royal Meteorol. Soc.*, 2005, **131**, 3583–3604.
9. Bertino, L. *et al.*, TOPAZ final scientific report. Technical report 251 NERSC, Bergen, 2004.
10. Heimbach, P., The MITgcm/ECCO adjoint modeling infrastructure. *CLIVAR Exchanges*, 2008, **44**, 13–17.
11. Oke, P. R., Brassington, G. B., Cummings, J., Martin, M. and Hernandez, F., GODAE inter-comparisons in the Tasman and Coral Seas. *J. Oper. Oceanogr.*, 2012, **5**, 11–24.
12. Kurian, J. and Vinayachandran, P. N., Mechanisms of formation of the Arabian Sea mini warm pool in a high resolution OGCM. *J. Geophys. Res.*, 2007, **112**, C05009; doi:10.1029/2006JC003631.
13. Vinayachandran, P. N., Kurian, J. and Neema, C. P., Indian Ocean response to anomalous conditions in 2006. *Geophys. Res. Lett.*, 2007, **34**, L15602; doi: 10.1029/2007GL030194.
14. Vinayachandran, P. N., Neema, C. P., Mathew, S. and Remya, R., Mechanisms of summer intraseasonal sea surface temperature oscillations in the Bay of Bengal. *J. Geophys. Res.*, 2012, **117**, C01005, doi: 10.1029/2011JC007433.
15. International CLIVAR Project Office, Understanding the role of the Indian Ocean in the climate system – implementation plan for sustained observations. CLIVAR Publication Series No. 100, January 2006.
16. Haidvogel, D. B., Arango, H. G., Hedstrom, K., Beckmann, A., Malanotte-Rizzoli, P. and Shchepetkin, A. F., Model evaluation experiments in the North Atlantic Basin: simulations in nonlinear terrain-following coordinates. *Dyn. Atmos. Oceans*, 2000, **32**, 239–281.
17. Shchepetkin, A. F. and McWilliams, J. C., The regional ocean modeling system (ROMS): A split-explicit, free-surface, topography-following-coordinate oceanic model. *Ocean Model.*, 2005, **9/4**, 347–404; doi: 10.1016/j.ocemod.2004.08.002.
18. Song, Y. and Haidvogel, D. B., A semi-implicit ocean circulation model using a generalized topography-following coordinate system. *J. Comp. Phys.*, 1994, **115**, 228–244.
19. Antonov, J. I. *et al.*, *World Ocean Atlas 2009, Volume 2: Salinity*. (ed. Levitus, S.), NOAA Atlas NESDIS 69, US Government Printing Office, Washington, DC, 2010, p. 184.
20. Locarnini, R. A. *et al.*, *World Ocean Atlas 2009, Volume 1: Temperature* (ed. Levitus, S.), NOAA Atlas NESDIS 68, US Government Printing Office, Washington, DC, 2010, p. 184.
21. Large, W. G., McWilliams, J. C. and Doney, S. C., Oceanic vertical mixing: a review and a model with a nonlocal boundary layer parameterization. *Rev. Geophys.*, 1994, **32**, 363–403.
22. Griffies, S. M. and Hallberg, R. W., Biharmonic friction with a Smagorinsky-like viscosity for use in large-scale eddy-permitting Ocean models. *Mon. Weather Rev.*, 2000, **128**, 2935–2946; doi: http://dx.doi.org/10.1175/1520-0493(2000)128<2935:BFWASL>2.0.CO;2.

23. Fairall, C. W., Bradley, E. F., Rogers, D. P., Edson, J. B. and Young, G. S., Bulk parameterization of air–sea fluxes for TOGA COARE. *J. Geophys. Res*., 1996, **101**, 3747–3764.
24. Yu, L. and Weller, R. A., Objectively analyzed air–sea heat fluxes for the global ice-free oceans (1981–2005). *Bull. Am. Meteorol. Soc*., 2007, **88**, 527–539.
25. Kummerow, C., Barnes, W., Kozu, T., Shiue, J. and Simpson, J., The tropical rainfall measuring mission (TRMM) sensor package. *J. Atmos. Ocean. Technol.*, 1998, **15**, 809–817.
26. Wentz, F. J., Gentemann, C. L., Smith, D. K. and Chelton, D. B., Satellite measurements of sea-surface temperature through clouds. *Science*, 2000, **288**, 847–850.
27. McPhaden, M. J. *et al.*, Supplement to RAMA: The Research Moored Array for African–Asian–Australian Monsoon Analysis and Prediction. *Bull. Am. Meteorol. Soc.*, 2009, **90**, ES5–ES8; doi: http://dx.doi.org/10.1175/2008BAMS2608.2.
28. Amol, P. *et al*., Observational evidence from direct current measurements for propagation of remotely forced waves on the shelf off the west coast of India. *J. Geophys. Res. C*, 2012, **117**; 2012, **15**, C05017; doi: 10.1029/2011JC007606.
29. Arnone, R. A., Satellite derived colour–temperature relationship in the Arabian Sea. *Remote Sensing Environ.*, 1987, **23**, 417–437.
30. Nath, A. N. *et al.*, Satellite forecasting for marine fishery resources exploitation along Indian coast. *Interface*, 1992, **3**, 1–3.
31. Solanki, H. U., Raman, M., Kumari, B., Dwivedi, R. M. and Narain, A., Seasonal trends in the fishery resources off Gujarat: salient observations using NOAA–AVHRR. *Indian J. Mar. Sci*., 1998, **27**, 438–442.
32. Pradhan, Y. A., Rajawat, S. and Nayak, S. R., Application of IRS P4 OCM data to study the impact of tidal propagation on sediment dynamics in the Gulf of Kachchh. *Indian J. Mar. Sci.*, 2004, **33**, 129–137.
33. Olascoaga, M. J., Idrisi, N. and Romanou, A., Biophysical isopycnic-coordinate modelling of plankton dynamics in the Arabian Sea. *Ocean Modell.*, 2005, **8**, 55–80.
34. Gundersen, J. S., Gardner, W. D., Richardson, M. J. and Walsh, I. D., Effects of monsoons on the seasonal and spatial distributions of POC and chlorophyll in the Arabian Sea. *Deep-Sea Res. II*, 1998, **45**, 2103–2132.
35. Latasa, M. and Bidigare, R. R., A comparison of phytoplankton populations of the Arabian Sea during the spring intermonsoon and southwest monsoon of 1995 as described by HPLC-analyzed pigments. *Deep-Sea Res. II*, 1998, **45**, 2133–2170.
36. Garrison, D. L. *et al.*, Microbial food web structure in the Arabian Sea: a US JGOFS study. *Deep-Sea Res. II*, 2000, **47**, 1387–1422.
37. Schott, F., Monsoon response of the Somali current and associated upwelling. *Prog. Oceanogr.*, 1983, **12**, 357–381.
38. Schott, F. and Fieux, M., The Somali current in autumn 1984, before the onset of the north-east monsoon. *Nature*, 1985, **315**, 50–52.
39. McCreary, J. P. *et al.*, Influences of diurnal and intraseasonal forcing on mixed-layer and biological variability in the central Arabian Sea. *J. Geophys. Res*., 2001, **106**, 7139–7155.
40. Prasad, V. S., Mohandas, S., Gupta, M. D., Rajagopal, E. N. and Dutta, S. K., Implementation of upgraded global forecasting systems (T382L64 and T574L64) at NCMRWF, Technical Report: NCMR/TR/5/2011, National Centre for Medium Range Weather Forecast, New Delhi, 2011.
41. Trenary, L. L. and Han, W., Intraseasonal-to-interannual variability of south Indian Ocean sea level and thermocline: remote versus local forcing. *J. Phys. Oceanogr.*, 2012, **42**, 602–627; doi: http://dx.doi.org/10.1175/JPO-D-11-084.1.
42. Kara, A. B., Rochford, P. A. and Hurlburt, H. E., An optimal definition for ocean mixed layer depth. *J. Geophys. Res.*, 2000, **105**, 16803–16821.
43. Thomson, R. E. and Fine, I. V., Estimating mixed layer depth from oceanic profile data. *J. Atmos. Ocean. Technol.*, 2003, **20**, 319–329.
44. Wijesekera, H. W. and Gregg, M. C., Surface layer response to weak winds, westerly bursts, and rain squalls in the western Pacific warm pool. *J. Geophys. Res. C1*, 1996, **101**, 977–997; doi: 10.1029/95JC02553.
45. Bathen, K. H., On the seasonal changes in the depth of the mixed layer in the North Pacific Ocean. *J. Geophys. Res.*, 1972, **77**, 7138–7150.
46. Lukas, R. and Lindstrom, E., The mixed layer of the western equatorial Pacific Ocean. *J. Geophys. Res*., 1991, **96**, 3343–3357.
47. Richards, K. J., Inall, M. E. and Wells, N. C., The diurnal mixed layer and upper ocean heat budget in the western equatorial Pacific. *J. Geophys. Res.*, 1995, **100**, 6865–6879.

ACKNOWLEDGEMENTS. P.N.V. thanks the INDOMOD programme of INCOIS, MoES. We thank the developers of the ROMS model. The altimeter products were produced by SSALTO/DUCAS and distributed by AVISO with support from CNES (http://www.aviso.oceanobs.com/duacs/). The National Centre for Medium Range Weather Forecasting (NCMRWF), New Delhi is acknowledged for making the atmospheric analysis and forecast products available for the ROMS simulations/forecasts. The TAO Project Office of NOAA/PMEL is acknowledged for making RAMA moored buoy data available for the validation of forecasts. The TMI data used for the forecast validations are produced by remote sensing systems and sponsored by the NASA Earth Science MEaSUREs DISCOVER project. We also thank CSIR–NIO, Goa for providing the ADCP data off the coast of Goa for this study. Ferret free-ware and MATLAB were used for the figures.